Supplementary Material

Noninvasive two-photon optical biopsy of retinal fluorophores

Grazyna Palczewska[1,2], Jakub Boguslawski[3], Patrycjusz Stremplewski[4], Lukasz Kornaszewski[3], Jianye Zhang[2], Zhiqian Dong[1,2], Xiao-Xuan Liang[5,] Enrico Gratton[6], Alfred Vogel[5,#], Maciej Wojtkowski[3,#], Krzysztof Palczewski[2,7,8,#]

[1]Polgenix, Inc., Department of Medical Devices, Cleveland OH 44106

[2]Gavin Herbert Eye Institute, Department of Ophthalmology, University of California, Irvine, CA 92697

[3]International Centre for Translational Eye Research, Institute of Physical Chemistry, Polish Academy of Sciences, Warsaw, 01-224, Poland

[4]Faculty of Physics, Nicolaus Copernicus University, Torun, 87-100, Poland

[5]Institute of Biomedical Optics, University of Luebeck, Luebeck, 23562, Germany

[6]Department of Biomedical Engineering, University of California, Irvine, CA 92697

[7]Department of Physiology,University of California, Irvine, CA 92697

[8]Department of Chemistry, University of California, Irvine, CA 92697

Keywords: retina, RPE, two-photon excitation, mouse models, phasor FLIM, hyperspectral imaging

[#]To whom correspondence should be addressed: Krzysztof Palczewski, Ph.D.: Gavin Herbert Eye Institute, Department of Ophthalmology, University of California, Irvine, CA 92657; kpalczew@uci.edu; Tel: (949) 824-6527; Fax: 949-824-4015

Maciej Wojtkowski, Ph.D.: Department of Physical Chemistry of Biological Systems, Institute of Physical Chemistry, Polish Academy of Sciences, Warsaw, Poland; mwojtkowski@ichf.edu.pl; Tel: +48-22-343-3283

Alfred Vogel, Ph.D.: Institute of Biomedical Optics, University of Luebeck, Peter-Monnik-Weg 4, 23562 Luebeck, Germany; alfred.vogel@uni-luebeck.de; Tel. +49-451-3101 3223

www.pnas.org/cgi/doi/10.1073/pnas.2007527117

SUPPLEMENTARY VIDEO

Video shows a series of images and sections along the RPE Z –axis from the intact eye of a 6.5-month-old albino *Abca4*$^{PV/PV}$*Rdh8*$^{-/-}$ mouse. Basal side of RPE is at Z=0 µm. Arbitrary colors are assigned as per the rainbow bar in the semicircle phasor plot shown in **SI Appendix**, **Fig. S3**.

METHODS

TPE imaging

To image mouse eye with the newly redesigned imaging system, pulsing IR light from a mode-locked Ti:sapphire pulsing laser after passing through a dispersion pre-compensation system and pulse selection system, was attenuated in a controlled, variable manner by using an electro-optic modulator (EOM) and directed to the scanners in the Leica TCSSP8 microscope. The horizontal scanning together with the vertical beam scanning spanned the imaged sample at typically 1.3 s per frame resulting in 256 by 256 or 512 by 512 pixel images (1). During imaging, to minimize sample exposure to laser light while detection was in the idle state, the EOM switched off the excitation beam on the return scan yielding a 62% duty cycle. Characterization of the fluorescence as a function of light power at the sample plane was obtained with a 100% duty cycle. In two-photon excitation imaging there is no need for de-scanning and a pinhole, because fluorescence photons are generated only within the vicinity of the focal spot, thus to minimize losses of the fluorescent light, imaging was preferentially done with the photon counting detector in a non-descanned configuration (NDD). Fluorescence was separated from the excitation light by the dichroic mirror which transmitted wavelengths longer than 670 nm and reflected shorter ones. Additionally, a blocking short pass filter which transmitted wavelengths shorter than 670 nm was placed in front of the NDD. A 1.0 NA 20x Leica objective was used for *ex vivo* imaging of enucleated, intact mouse eyes submerged in phosphate–buffered saline (PBS) composed of 9.5 mM sodium phosphate, 137 mM NaCl and 2.7 mM KCl, pH 7.4. For *in vivo* imaging, an anesthetized mouse was surrounded by a heating pad and placed on a mechanical stage with its eye covered with GenTeal gel and a thin 3.2 mm diameter, 0 diopter contact lens (Cantor and Nissel, Northamptonshire, UK) to avoid drying the cornea. To efficiently couple excitation light and capture fluorescence from the retina and RPE, light was guided into the eye and finely

focused on the retina with the use of a custom designed periscope objective which provided a nearly collimated light beam at the contact lens surface. Furthermore, the periscope facilitated an adjustable degree of divergence of the light beam to compensate for variable refractive errors of the mouse eyes and to enable selection of the depth of interest (2). To reduce a vignetting effect, we modified the periscope objective design. The new optical relay reduced the beam diameter to 1.9 mm instead of 2.4 mm as in the old design. It also provided a higher quality beam with a field of view of 22 degrees. The scale bars for *in vivo* images were obtained using the scaling factor of 1.9 +/- 0.3, obtained by comparing the dimensions of RPE cells *ex vivo* using a 1.0 NA 20x Leica objective with those obtained *in vivo* with the periscope objective.

Fluorescence lifetime imaging (FLIM)

To collect and analize FLIM data we used modified Leica TCS SP8 microscope with Falcon architecture (3), equipped with a Ti:saphire pulsing laser as described above and low-noise actively-cooled photon-counting hybrid detectors (HyD) with a GaAsP photocathode (**Fig. 1**). In addition to high sensitivity, the HyD has a faster single electron response, less than 600 ps, compared to a high-end Hamamatsu PMT, typically 1 ns. The detector was placed in a nondescanned (NDD) configuration. With each laser pulse, a fast photodiode PicoQuant TDA200 placed after the beam splitter provided the synchronization signal for photon detection. The synchronization signal and signals from the photon detector were digitized and analyzed using the field-programmable gate array (FPGA) (3). For each pixel, the lifetime decay data were collected by measuring photon arrival time as the difference between each photon detection event and the corresponding excitation pulse. Fluorescence excitation light was adjusted to avoid detector pile-up and yet enable collection of approximately 1000 photons per pixel in no more than 60 s data collection time in the area of interest. This approach enabled formation of FLIM images. In the FLIM approach to data analyses, an artificial color scale was based on mean photon arrival times for each pixel, furthermore, software-based arrival time filtering (time gating) was used in some cases to increase contrast of selected fluorophores of interest. Amplitude weighted mean fluorescence lifetime (τ_m) of synthetic standards was obtained using equation S1 (4).

$$\tau_m = (A_1 \cdot \tau_1 + A_2 \cdot \tau_2 + A_3 \cdot \tau_3)/(A_1 + A_2 + A_3), \quad \text{(S1)}$$

where the coefficients A_i and τ_i represent amplitudes and lifetimes based on the approximation of fluorescence decay (F) by the sum of 1, 2 or 3 exponent functions, such that $F=A_1 \cdot e^{-t/\tau_1} + A_2 \cdot e^{-t/\tau_2} + A_3 \cdot e^{-t/\tau_3}$.

However, to analize the subcellular distribution of retinal fluorophores based on the FLIM data, the false color scale for FLIM imaging was predominantly assigned based on the phasor approach. To form phasor plots the data for each imaging pixel were converted from the time domain to phase domain using the phasor transformation equations S2 (5, 6).

$$g_{i,j} = \int_0^T I_{i,j}(t) \cdot \cos(2\pi \cdot PRF \cdot t)\, dt \Big/ \int_0^T I_{i,j}(t) dt$$

$$s_{i,j} = \int_0^T I_{i,j}(t) \cdot \sin(2\pi \cdot PRF \cdot t)\, dt \Big/ \int_0^T I_{i,j}(t) dt \qquad \text{(S2)}$$

Where $g_{i,j}$ and $s_{i,j}$ are the X and Y coordinates in the phasor plot, T is the period of the pulsing light at selected PRF, PRF is the excitation light PRF and *i, j* are the X and Y coordinates of pixel in the original microscopy image. In this approach fluorescence decay data are represented by points on a universal semicircle, such that the decay data for each pixel are represented by a point on the phasor plot (**Fig. 1**) (7). Thus image pixels with the same decay characteristics are represented as points with the same X, Y coordinates in the semicircle phasor plot. The X, Y coordinates on the semicircle plot can be expressed by $g_{i,j} = m_{i,j} \cdot \cos(\Phi_{i,j})$ and $s_{i,j} = m_{i,j} \cdot \sin(\Phi_{i,j})$, respectively, whereby $m_{i,j}$ and $\Phi_{i,j}$ are the modulation and phase at the image pixel i,j. If the phasor point is located on the line of the universal semicircle, it can be assigned a mono-exponential FLIM (τ), following the formula $\tan(\Phi) = 2\pi \cdot PRF \cdot \tau$, where Φ is the angle on the phasor plot (**Fig. 1C**). Furthermore, the longer lifetimes are represented by the larger phase angle than the shorter lifetimes. For PRF=80 MHz, Φ=0 degree and Φ=90 degree on the universal semicirle phasor plot correspond accordingly to 0 and 12.5 ns. Multi-exponential lifetimes are located inside the universal semicircle and represent linear combinations of their components (6). Phasor FLIM analyses start by displaying the data points on the 2D graph, universal semicircle and then selecting clusters of points of lifetime distributions. These procedures are followed by the interpretation of the corresponding phasor FLIM image. For FLIM analyses we used Leica LAS X FLIM Version 3.5.5 software and the ImageJ Version 1.51 analyze particle tool.

Retinyl esters analysis

Samples were collected and homogenized in 1 ml of sodium phosphate buffer, 10 mM, pH 8.0, containing 50% methanol (v/v) and 100 mM hydroxylamine. Then 2 ml of sodium chloride (5 M) were added. The resulting mixture was extracted with 3.5 ml of ethyl acetate twice. The combined organic layers were dried *in vacuo*, reconstituted in 400 µl of hexane, and 100 µl of the extract were injected into a normal-phase high-performance liquid chromatography (HPLC) column (Agilent Sil, 5 µm, 4.6 × 250 mm; Agilent Technologies, Santa Clara, CA) in a stepwise gradient

of ethyl acetate in hexanes (0–17 min, 0.6%; 17.01–30 minutes, 10%) at a flow rate of 1.4 $ml \cdot min^{-1}$. Retinoids were detected by monitoring absorbance at 325 nm and quantified based on a standard curve representing the relationship between the amount of synthetic retinoid standard and the area under the corresponding chromatographic peak.

Synthetic fluorescence standards

Fluorescein was purchased from Fisher Scientific, catalogue number F1300, and a solution in sodium borate, pH 9.5, was used for experiments. Sigma Aldrich retinyl palmitate was purchased from Fisher Scientific, catalogue number NC1186485. A2E was synthesized from ethanolamine and all-*trans*-retinal as previously described (8). Fluorescence spectra and lifetime characterizations were done after placing a sample on a hanging drop slide.

FIGURES

Fig. S1.

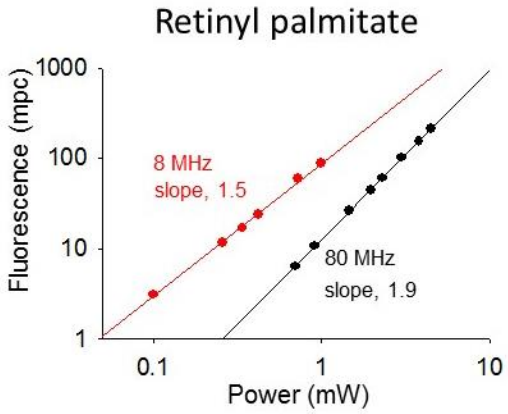

Fig. S1. **Fluorescence of retinyl palmitate as a function of excitation light power.** Data were acquired using 750 nm excitation light and a 1.0 NA objective. PRF and slope of the linear regression lines through data points are indicated.

Fig. S2.

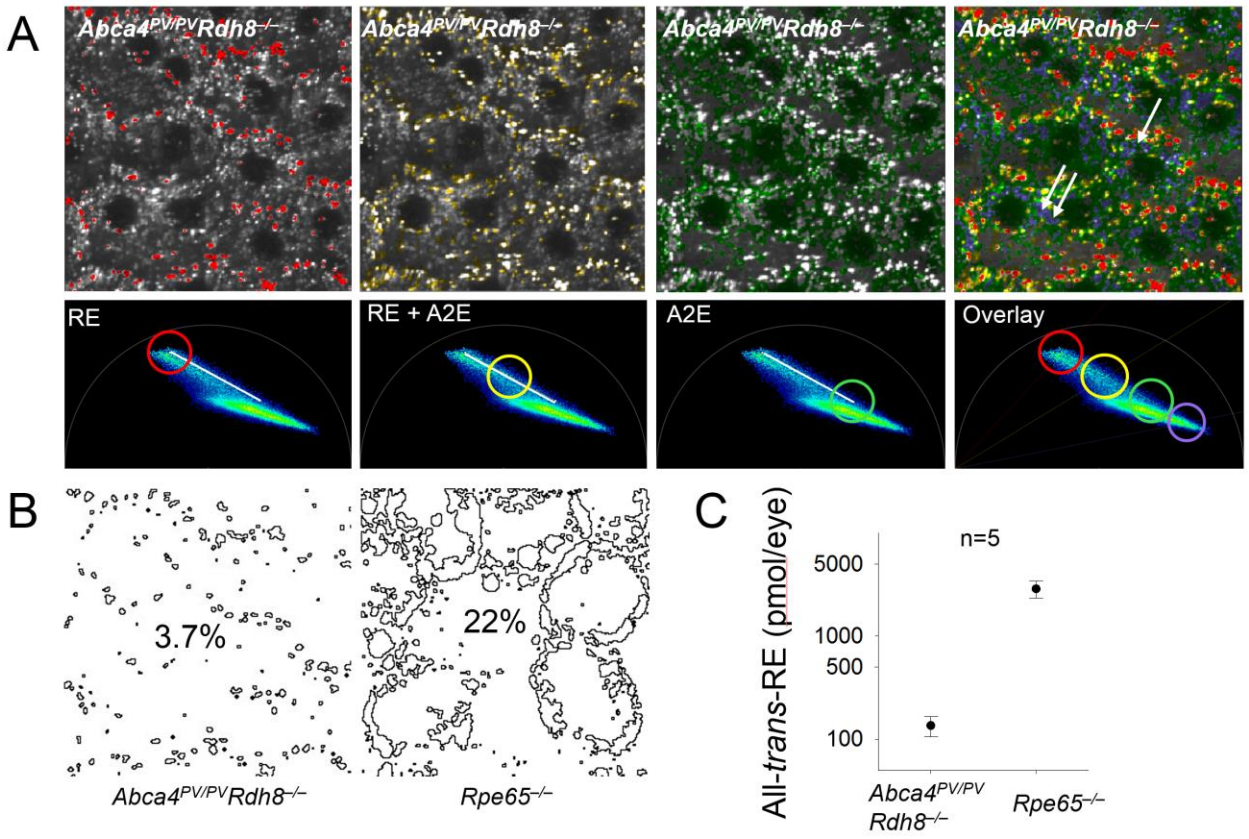

Fig. S2. **Quantification of retinyl ester in the RPE of an intact eye.** Retinyl ester and A2E content and distribution in the RPE based on Phasor FLIM of the intact eyes from a 3.5-month-old albino *Abca4*$^{PV/PV}$*Rdh8*$^{-/-}$ mouse and a 6-month-old albino *Rpe65*$^{-/-}$ mouse with 730 nm TPE. A) Top row, phasor FLIM images and bottom row, phasor plots in *Abca4*$^{PV/PV}$*Rdh8*$^{-/-}$ mouse RPE. In FLIM images the color mask is based on the arbitrary color assignments in phasor plots. Red circle outlines a grouping of points in the region of the retinyl esters (RE) phasor cluster as in **Fig. 2A**; green circle outlines phasor points with A2E-like properties; yellow circle outlines points with contributions from both fluorophores, and purple circle outlines points with life-times shorter than outlined by green circle. Yellow circle lies halfway on the white line joining the phasor points for A2E and RE. White arrows indicate some of the purple granules whose location overlaps with those of 850 nm excited A2E granules in **Fig. 2B**. B) Phasor mask followed by ImageJ-based quantification of the area occupied by retinosomes; percentage of area occupied by retinosomes is indicated in each panel. C) Quantification of retinyl esters by HPLC analyses. Bars indicate standard deviation, n=5 animals.

Fig. S3.

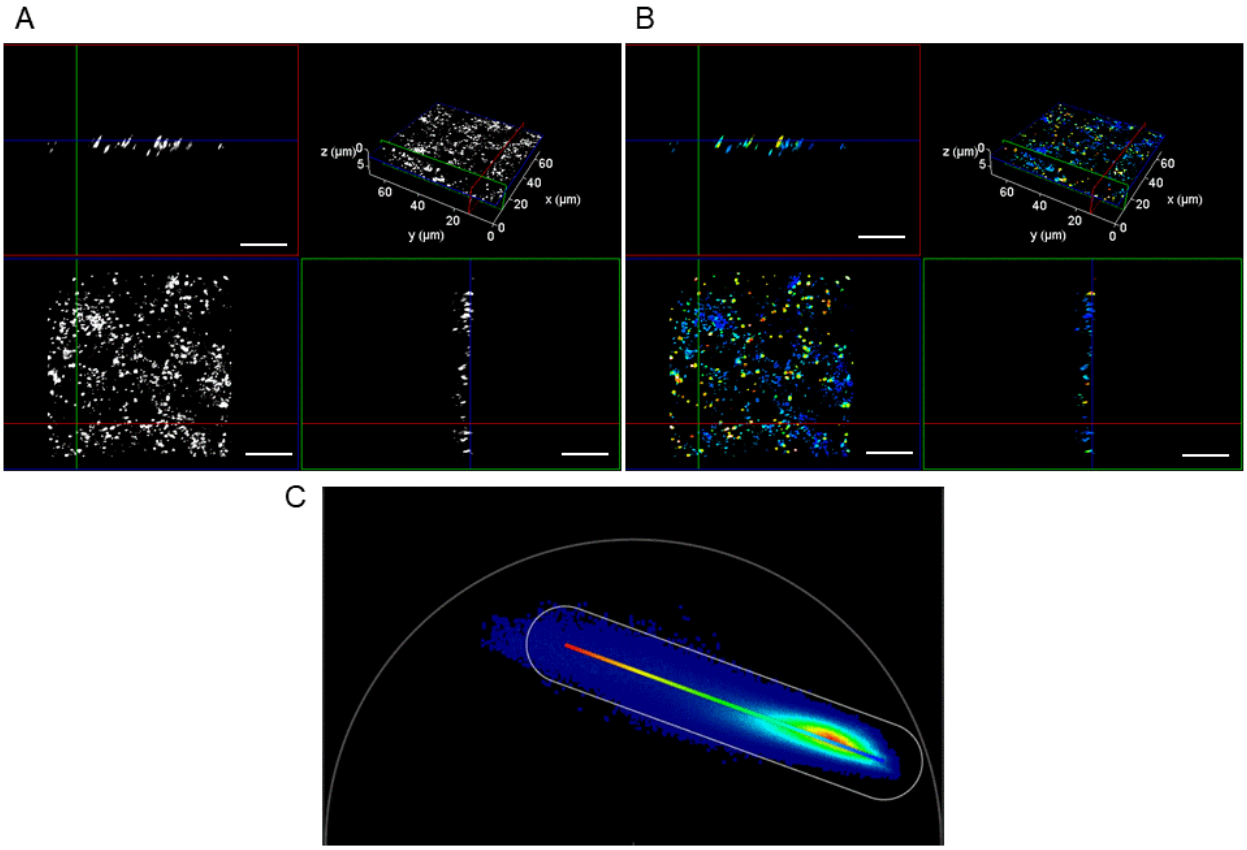

Fig. S3. Distribution of retinyl esters and retinal condensation products in the RPE of the intact mouse eye. In A and B, upper left corner shows Z-axis section along plane outlined in faint red in 3D visualization shown in the upper right corner; lower left corner shows *en face* image of RPE at Z-axis value as indicated by faint blue line in upper right corner; and lower right corner shows Z-axis section along plane outlined in faint green in 3D visualization shown in upper right corner. A) Fluorescence intensity-based sections and 3D –visualization of fluorophores of the RPE in the intact eye of a 6.5-month-old albino *Abca4*$^{PV/PV}$*Rdh8*$^{-/-}$ mouse. B) Phasor FLIM sections and 3D – visualization based on arbitrary color scale represented by the rainbow bar in C. C) Semicircle phasor plot is shown from the entire z-stack. Basal side of RPE is at z=0 µm. Scale bars, 20 µm.

Fig. S4.

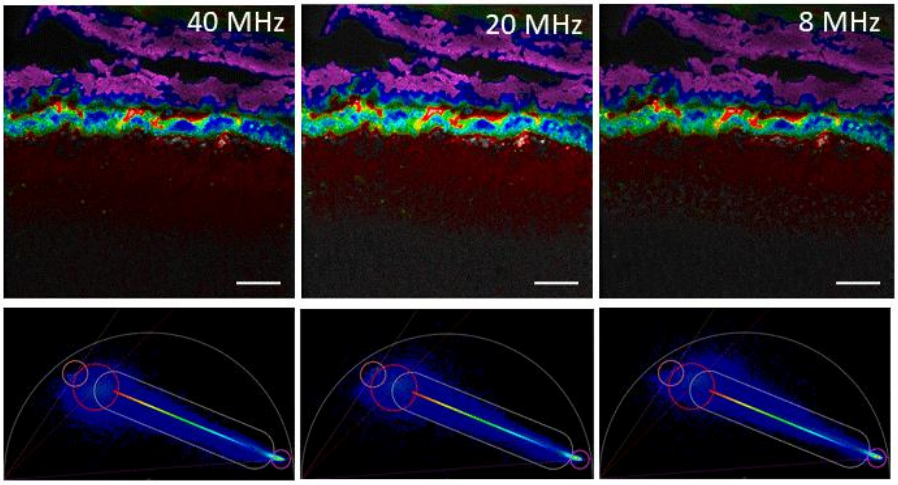

Fig. S4. FLIM based on phasor analyses does not change with pulse repetition frequencies (PRF). PRF are indicated in each image of the section from black *Rpe65*$^{-/-}$ mice. Arbitrary colors in phasor FLIM images (upper row) based on rainbow bars and color circles in phasor plots (bottom row). Scale bars, 20 µm.

Fig. S5.

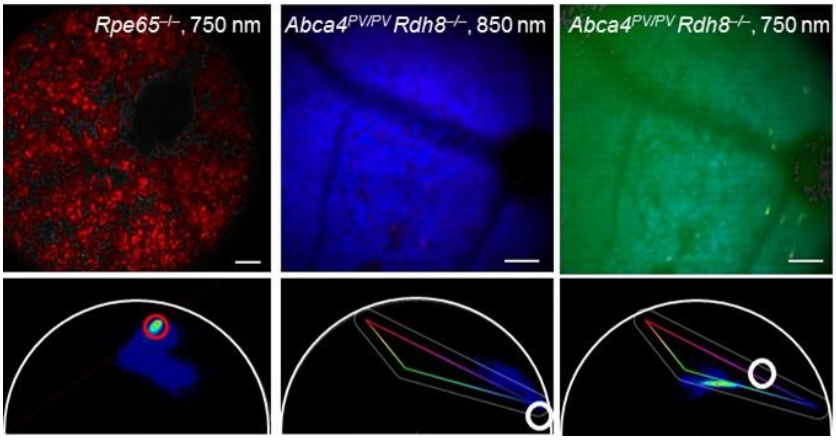

Fig. S5. Fluorophores in the RPE of live 7-month-old albino mice. Top row, phasor FLIM of live *Rpe65*$^{-/-}$ and *Abca4*$^{PV/PV}$*Rdh8*$^{-/-}$ mice. Genotype and excitation wavelengths are indicated in each panel. Bottom row phasor plots. Arbitrary color in *Rpe65*$^{-/-}$ are based on the red circle in the phasor plot. Arbitrary colors in *Abca4*$^{PV/PV}$*Rdh8*$^{-/-}$ mice are based on the rainbow triangle like the one shown in Fig. 2. White circles indicate locations of phasor points of 10 mM A2E in Fig. 1. Scale bars, 100 µm.

Fig. S6.

.

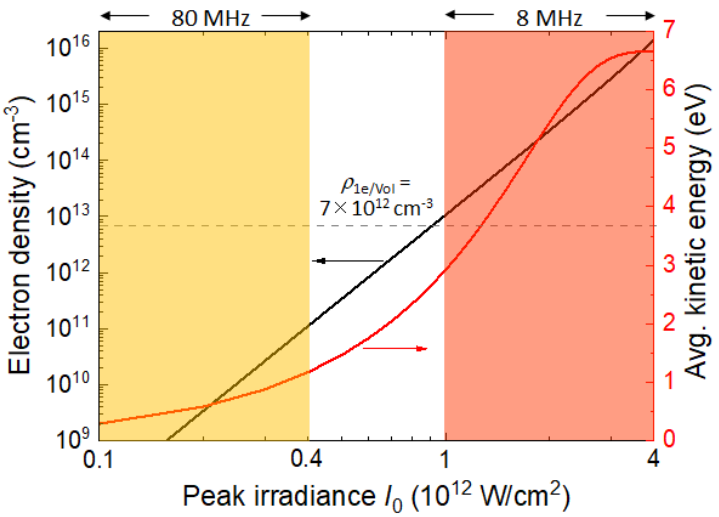

Fig. S6. CB electron density and average kinetic energy, ε_{avg}, as a function of peak laser irradiance. The dashed line indicates the electron density, at which one free electron per focal volume is produced by each laser pulse.

Fig. S7.

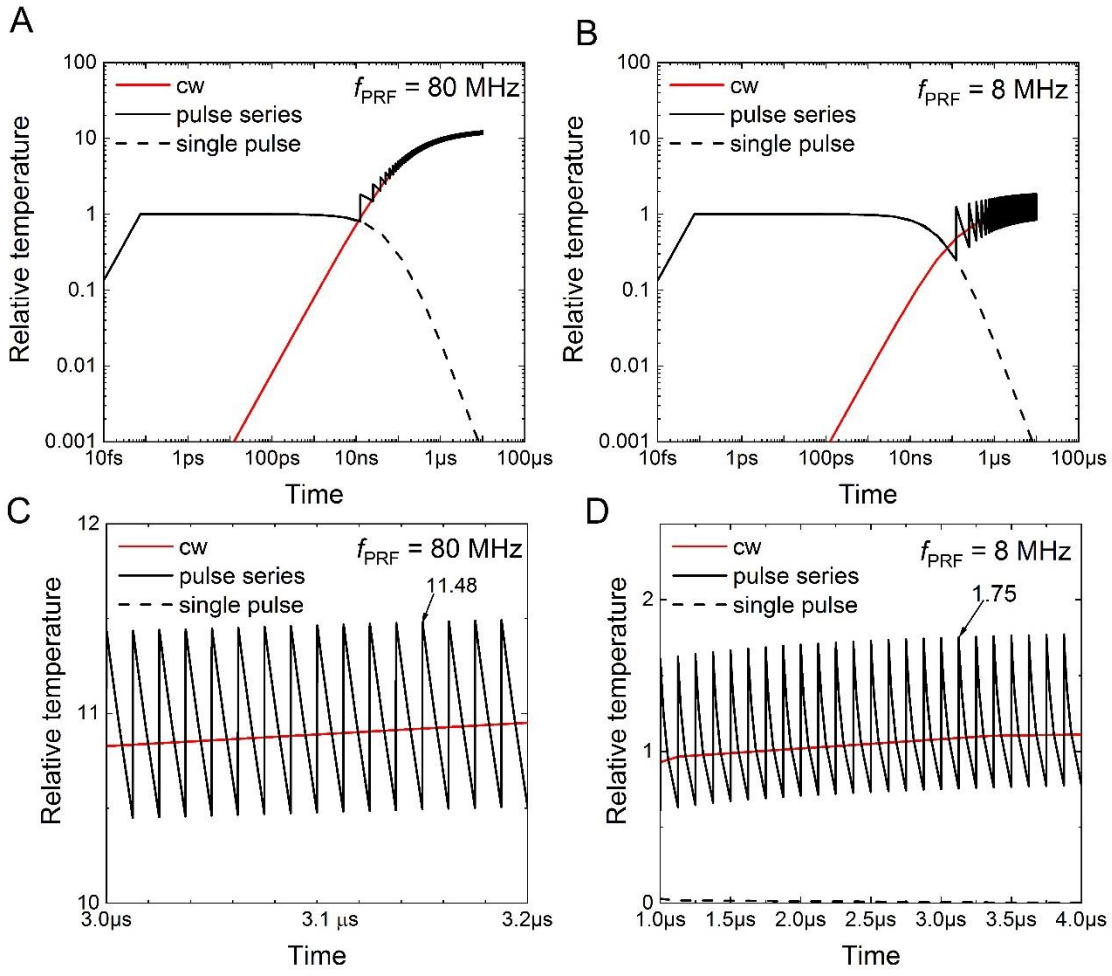

Fig. S7. Temperature accumulation during fs laser pulse trains. The cumulative temperature rise during fs pulse trains is shown in **A** and **C** for 80-MHz PRF, and in **B** and **D** for 8 MHz. Temperature values are normalized to the temperature jump ΔT_{pulse} produced by a single pulse. Heat accumulation factors at the end of the pixel dwell time are indicated in the enlarged portions of the $T(t)$ curves in C and D.

Table S1 Temperature increase in melanosomes of 300 nm radius by single pulses and pulse series at the average power values used for two-photon retinal imaging at 8 MHz and 80 MHz. Values corresponding to the parameters used for imaging at the respective pulse repetition frequencies are marked in red.

f_{PRF}	ΔT(K) 1.8 mW	ΔT(K) 3.5 mW
8-MHz Single pulse	45.6	88.7
80-MHz Single pulse	4.56	8.9
8-MHz Pulse series	79.8	155.3
80-MHz Pulse series	52.5	102.1
cw	49.7	96.7

References

1. Palczewska G, Kern TS, & Palczewski K (2019) Noninvasive Two-Photon Microscopy Imaging of Mouse Retina and Retinal Pigment Epithelium. *Methods Mol Biol* 1834:333-343.
2. Stremplewski P, Komar K, Palczewski K, Wojtkowski M, & Palczewska G (2015) Periscope for noninvasive two-photon imaging of murine retina in vivo. *Biomed Opt Express* 6(9):3352-3361.
3. Alvarez LAJ*, et al.* (2019) SP8 FALCON: a novel concept in fluorescence lifetime imaging enabling video-rate confocal FLIM. *Nat Methods* 16(10).
4. Sauer L*, et al.* (2018) Review of clinical approaches in fluorescence lifetime imaging ophthalmoscopy (Erratum). *J Biomed Opt* 23(9):1.
5. Digman MA, Caiolfa VR, Zamai M, & Gratton E (2008) The phasor approach to fluorescence lifetime imaging analysis. *Biophys J* 94(2):L14-16.
6. Ranjit S, Datta R, Dvornikov A, & Gratton E (2019) Multicomponent Analysis of Phasor Plot in a Single Pixel to Calculate Changes of Metabolic Trajectory in Biological Systems. *J Phys Chem A* 123(45):9865-9873.
7. Birks JB, Munro IH, & Dyson DJ (1963) Excimer Fluorescence .2. Lifetime Studies of Pyrene Solutions. *Proc R Soc Lon Ser-A* 275(1360):575-+.
8. Parish CA, Hashimoto M, Nakanishi K, Dillon J, & Sparrow J (1998) Isolation and one-step preparation of A2E and iso-A2E, fluorophores from human retinal pigment epithelium. *Proc Natl Acad Sci U S A* 95(25):14609-14613.